Nanoscale Horizons

ROYAL SOCIETY OF CHEMISTRY

COMMUNICATION

View Article Online
View Journal | View Issue

Check for updates

Cite this: *Nanoscale Horiz.*, 2022, 7, 899

Received 27th March 2022,
Accepted 30th May 2022

DOI: 10.1039/d2nh00152g

rsc.li/nanoscale-horizons

Published on 30 May 2022. Downloaded on 8/22/2025 4:03:11 PM.

A sodiophilic VN interlayer stabilizing a Na metal anode†

Xianming Xia,[a] Xiang Lv,[a] Yu Yao,[b] Dong Chen,[a] Fang Tang,[a] Lin Liu,[a] Yuezhan Feng,[c] Xianhong Rui *[a] and Yan Yu *[b]

Sodium (Na) metal is a very encouraging anode material for next-generation rechargeable batteries owing to its high specific capacity, earth-abundance and low-cost. However, the application of Na metal anodes (SMAs) is hampered by dendrite growth and "dead" Na formation caused by the uncontrollable Na deposition, leading to poor cycle life and even safety concerns. Herein, a high-performance Na anode is designed by introducing an artificial VN interlayer on the Na metal surface (Na/VN) by a simple mechanical rolling process to regulate Na nucleation/deposition behaviors. The density functional theory (DFT) and experiment results uncover that the VN possesses high "sodiophilicity", which can facilitate the initially homogeneous Na nucleation and cause Na to distribute evenly on the VN interlayer. Therefore, uniform Na deposition with dendrite-free morphology and prolonged cycling lifespan (over 1060 h at 0.5 mA cm^{-2}/1 mA h cm^{-2}) can be realized. Moreover, the full cell assembled by coupling a $Na_3V_2(PO_4)_3$ (NVP) cathode and Na/VN anode presents superior cycling performance (*e.g.*, 96% capacity retention even after 800 cycles at 5C). This work provides a promising direction for regulating Na nucleation and deposition to achieve dendrite-free metal anodes.

New concepts

Controllable and homogeneous Na deposition plays a critical role for dendrite-free sodium metal anodes (SMAs). In this work, we introduce an artificial VN interlayer on the surface of Na metal *via* a simple and effective mechanical rolling process to regulate the initial Na nucleation and subsequent homogeneous plating, aiming to achieve dendrite-free SMAs. Density functional theory calculations demonstrate that VN has high sodiophilicity, which can induce Na ion fast adsorption and uniform nucleation. Furthermore, experimental results further verify that the artificial VN interlayer helps to decrease the Na ion nucleation overpotential and possesses fast interfacial charge transfer kinetics, promoting homogeneous Na deposition. This work improves the cycling stability of SMAs *via* introducing a sodiophilic artificial VN interlayer, which provides promising insights into dendrite-free SMAs.

Introduction

With rechargeable battery technologies rapidly becoming applicable in electric vehicles and industrial systems in recent years, their energy density and cost have become the primary concerns for energy storage.[1–4] It is reported that employing active metals (such as Li, Na, Zn and K) as anodes directly is a hopeful method to significantly enhance the energy density of batteries.[5–14] Among them, the sodium metal anode (SMA) has attracted great interest benefiting from its high theoretical capacity (1166 mA h g^{-1}), low redox potential (−2.71 V *vs.* standard hydrogen electrode) and cost-effectiveness.[15–20] However, the practical application of SMAs is crucially hampered by dendrite growth and "dead" Na generation, which are principally derived from the uncontrolled Na deposition, leading to poor Coulombic efficiency, short cycle lifespan and even safety issues.

In principle, the initial nucleation of Na plays a critically important role for the subsequent depositing behavior and the ultimate morphology characteristics of Na metal.[21,22] Thus, considerable research articles have been dedicated to regulating the initial Na nucleation behavior for dendrite-free SMAs. One of the effective approaches is physical implantation of nucleation seeds which can react with metal Na to form Na-rich alloys, benefiting the initial Na nucleation at specific sites. For instance, Wang *et al.* designed well-dispersed Sn nanoparticles to guide initial Na nucleation (formation of $Na_{15}Sn_4$ alloy), enabling highly reversible and dendrite-free SMAs.[23] Afterwards, several other metal nanoparticles (*e.g.*, Sb,

[a] *School of Materials and Energy, Guangdong University of Technology, Guangzhou 510006, China. E-mail: xhrui@gdut.edu.cn*
[b] *Hefei National Laboratory for Physical Sciences at the Microscale, Department of Materials Science and Engineering, Key Laboratory of Materials for Energy Conversion, Chinese Academy of Sciences (CAS), University of Science and Technology of China, Hefei, Anhui 230026, China. E-mail: yanyumse@ustc.edu.cn*
[c] *Key Laboratory of Materials Processing and Mold (Ministry of Education), Zhengzhou University, Zhengzhou 450002, China*

† Electronic supplementary information (ESI) available. See DOI: https://doi.org/10.1039/d2nh00152g

Published on 30 May 2022. Downloaded on 8/22/2025 4:03:11 PM.

Zn, and Ag) have been employed as the alloyed seeds to induce the initially uniform Na nucleation.[24–29] However, the repetitive alloying–dealloying during the plating/stripping processes leads to the exfoliation of the sodiophilic metal nanomaterials, thus limiting the cycling stability (generally less than 300 h).

To enhance the cycling performance, researchers have designed sodiophilic seed materials without the occurrence of alloying–dealloying reaction during the Na plating/stripping process.[30] For example, Xie *et al.* designed well-dispersed Co nanoparticles encapsulated in porous nitrogen-doped carbon rhombic dodecahedra to regulate Na nucleation and deposition.[31] Wang's group constructed sodiophilic nitrogen (N) and sulfur (S) co-doped carbon nanotube (NSCNT) paper to adjust the initial Na nucleation, displaying dendrite-free and flat morphology during the reiterative Na stripping and plating processes, resulting in outstanding cycling stability.[32] Although these reports shed light on regulating initially homogeneous Na nucleation for dendrite-free SMAs, complicated fabrication processes such as predeposition and disassembly/reassembly are always involved. In addition, the lifespan is still less than 500 h and the rate performance is generally poor, especially in carbonate-based electrolytes. Therefore, introducing a highly sodiophilic material that is simple to manipulate is still desired to produce highly reversible SMAs, especially at high current densities.

Herein, we develop a sodiophilic artificial VN interlayer on the surface of fresh Na metal foil (Na/VN) to accomplish homogeneous Na nucleation and deposition. The density functional theory (DFT) calculations demonstrate that the VN has high adsorption energy toward Na^+, and experimental results further reveal that a lower nucleation overpotential can be obtained for the SMA modified by an artificial VN interlayer. High sodiophilicity and lowing nucleation barrier of the VN interlayer can promote the initial Na nucleation and conduct Na to deposit evenly without dendrite formation. Consequently, the symmetric Na/VN‖Na/VN cell exhibits a prolonged lifespan of over 1060 h at 0.5 mA cm^{-2} and 670 h at 1.0 mA cm^{-2}. Furthermore, a full cell of Na/VN‖$Na_3V_2(PO_4)_3$ is constructed, which exhibits excellent rate performance and cycling stability (over 800 cycles even at 5C).

Results and discussion

Fig. 1a illustrates the preparation process of an artificial VN interlayer *via* rolling commercial VN powder (Fig. S1, ESI†) on the surface of fresh Na metal foil in an Ar-filled glovebox. After the modification, the surface of the Na metal foil changes from silvery to gray, as shown in optical images (Fig. S2, ESI†), suggesting the successful formation of an artificial layer (Na/VN). The morphology characteristic of the SMAs was researched *via* scanning electron microscopy (SEM). Fig. 1b demonstrates that, after coating of an artificial VN interlayer, the electrode surface becomes very smooth without potholes, and VN particles intimately contact together (Fig. 1c), facilitating the formation of a uniform Na ion concentration field on the surface. Furthermore, the images of energy-dispersive X-ray spectroscopy (EDS) mapping display the even distribution of V and N elements on the surface (Fig. S3, ESI†). The cross-sectional SEM image in Fig. S4 (ESI†) presents that the thickness of the artificial interlayer of VN is about 70 μm, and it is in close contact with the Na metal foil, which improves the structure stability and decreases the contact impedance.

X-ray diffraction (XRD) and transmission electron microscopy (TEM) were conducted to investigate the phase structure and chemical states of the artificial interlayer. It is clear in the XRD pattern that the phase structure of VN still remained, meaning that the VN does not react with Na during the rolling process (Fig. 1d). And it is notable that the broad peaks located at around 6 and 19 degrees are assigned to the polyimide tape that covered on Na/VN for protection (Fig. S5, ESI†). Moreover, it is clear that the Na/VN displays a similar morphology to that of the VN, *i.e.*, micron/submicron-sized particles (Fig. 1e). The corresponding selected area electron diffraction (SAED) pattern with diffraction rings can be indexed as (111), (200), (311) and (222) planes of cubic VN (JCPDS No. 73-0528), indicating that the Na/VN particles are polycrystalline (Fig. 1f). The elemental mapping images of an individual Na/VN particle further confirm the homogenous distribution of V and N, and it is uniformly surrounded by the Na (Fig. 1g). The high-resolution TEM analysis (Fig. 1h and Fig. S6, ESI†) further proves that the Na/VN is indeed polycrystalline, and the interplanar spacing of 0.20 and 0.23 nm corresponds to the (200) and (111) planes of VN, respectively. Additionally, the surface information and valence state of VN covered on Na metal foil were investigated by X-ray photoelectron spectroscopy (XPS), as exhibited in Fig. S7 (ESI†). The strong peaks at binding energies of 513.3 eV (V 2p) and 397.5 eV (N 1s) are assigned to V–N bonds.[33–37] These results indicate that VN can maintain the structure stability.

The electrochemical Na plating/stripping performance of the bare Na and Na/VN electrodes was studied in symmetric cells. As clearly displayed in Fig. 2a, the bare Na electrode presents a higher initial plating/stripping polarized voltage and shorter cycle lifespan with only 132 h at 0.5 mA cm^{-2} (Fig. S8a and b, ESI†), which may be due to the unstable Na plating/stripping causing the formation of Na dendrites, and then internal short circuiting. By contrast, the electrode modified by a VN artificial layer presents a lower polarized voltage and a long-term cycling stability over 1060 h (Fig. 2a and Fig. S8c, ESI†). Moreover, when the current density of Na plating/stripping is heightened to 1 mA cm^{-2}, the symmetric Na/VN cell also exhibits a lower and more stable initial voltage hysteresis (Fig. S9a, ESI†). And the symmetric Na/VN cell exhibits an exceptional cycling performance over 670 h (Fig. 2b and Fig. S9c, ESI†). However, signs of short circuiting are found after cycling for 116 h for the symmetric bare Na cell (Fig. 2b and Fig. S9b, ESI†). These results evidence that the artificial VN interlayer plays an important role for prolonging the cycling lifespan of the symmetric cell. Moreover, the voltage step is obvious in the symmetric Na/VN cell during plating and

 This journal is © The Royal Society of Chemistry 2022

Published on 30 May 2022. Downloaded on 8/22/2025 4:03:11 PM.

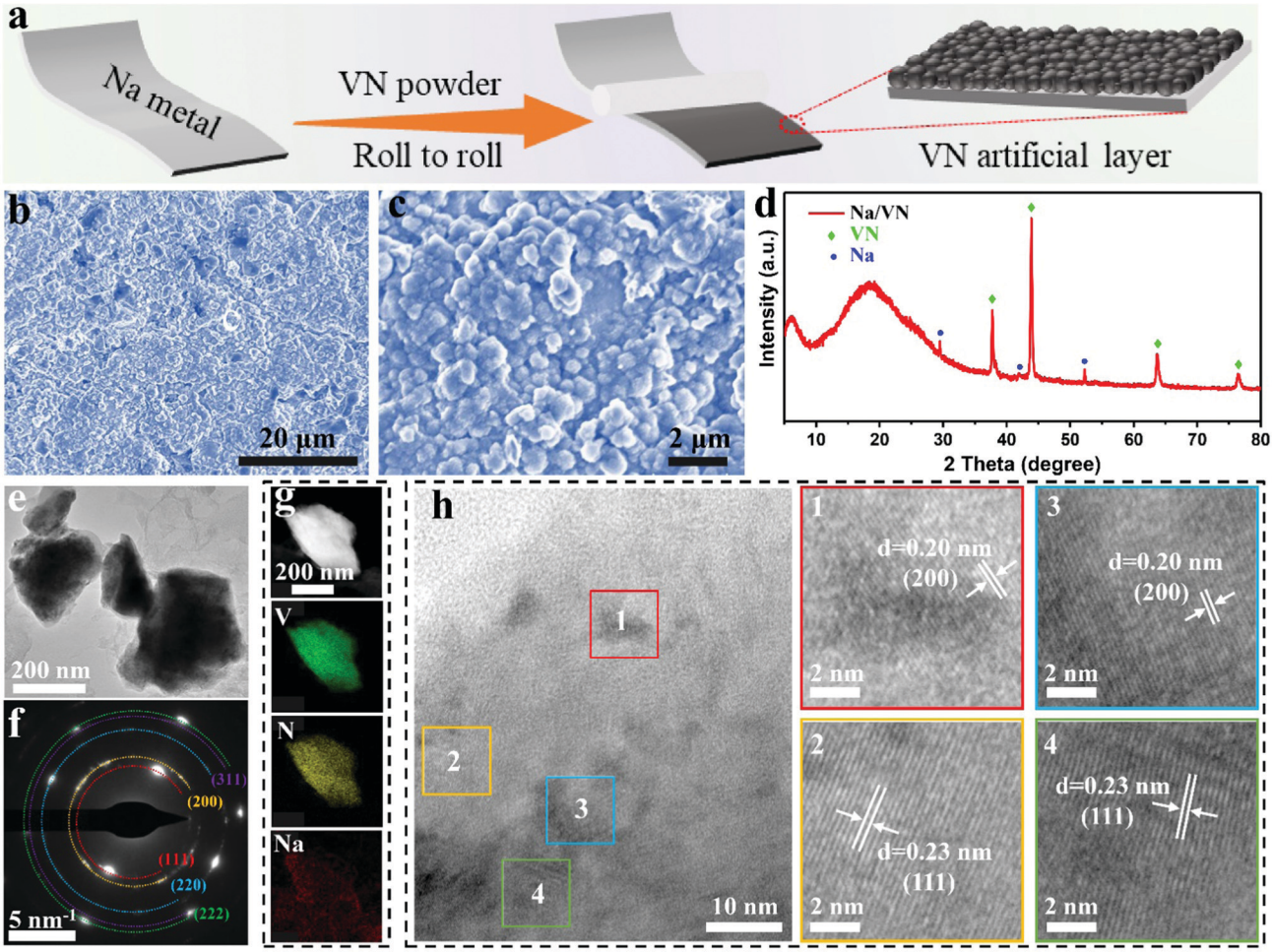

Fig. 1 (a) Illustration of the fabrication process of an artificial VN interlayer on the surface of Na metal foil. (b and c) SEM images of the Na/VN electrode. (d) XRD pattern of the Na/VN electrode. (e) TEM image, (f) SAED pattern, (g) HAADF-STEM image and corresponding elemental mapping and (h) HRTEM image of the Na/VN electrode.

stripping processes, while for the symmetric Na/VN cell, the voltage step exhibits a much lesser degree. This is attributed to a passivation layer (*i.e.*, VN) on the Na electrode, reducing the polarization.[38] Furthermore, to evaluate the potential application for sodium metal batteries, the rate performance of symmetric Na/VN and bare Na cells was investigated with a fixed capacity of 1 mA h cm^{-2}. As shown in Fig. 2c, when the current density of plating/stripping increases from 0.5 to 4 mA cm^{-2}, the Na/VN symmetric cell can still retain a steady voltage profile, indicating that the artificial VN interlayer achieves stable Na plating/stripping cycles. In contrast, the bare Na electrode shows a fluctuant voltage profile and high polarized voltage due to the ununiform Na deposition and the growth of Na dendrites, which significantly enhance the kinetic migration barrier. Furthermore, when compared with previously reported SMAs, the cycling performance of our Na/VN electrode at different current densities is still superior,[32,39–43] as shown in Fig. 2d. Therefore, it can be concluded that the artificial VN interlayer possesses high effectiveness for improving the rate performance and cycling life of SMAs.

The benefit of the VN interlayer toward Na deposition was also evaluated. Fig. 3a exhibits the voltage–time profiles of Na deposition for Na/VN and bare Na electrodes (current density: 0.5 mA cm^{-2}). It is easy to see that the Na nucleation overpotential for the bare Na electrode is calculated to be 68 mV. By contrast, the overpotential of the Na/VN is much lower (only 36 mV), indicating that the VN artificial interlayer has a smaller nucleation barrier, facilitating the homogeneous Na nucleation.[44] In addition, their Na deposition behaviours at different Na plating/stripping states were further studied *via ex situ* SEM characterizations (Fig. 3b). The surface of the Na/VN electrode at the initial state is relatively smooth, completely covered by VN particles (Fig. 3c and Fig. S10a, ESI†). With the areal capacity of plating Na reaches 0.5 mA h cm^{-2}, the particle size is visibly expanded (Fig. 3d and Fig. S10b, ESI†), which indicates that Na^+ ions incline to nucleate and deposit around the VN particle. When the plating Na further increases to 1.0 mA h cm^{-2}, a compact and smooth deposition layer can be formed and no Na dendrites are found (Fig. 3e and Fig. S10c, ESI†). Therefore, the nucleation guidance from the VN artificial

Published on 30 May 2022. Downloaded on 8/22/2025 4:03:11 PM.

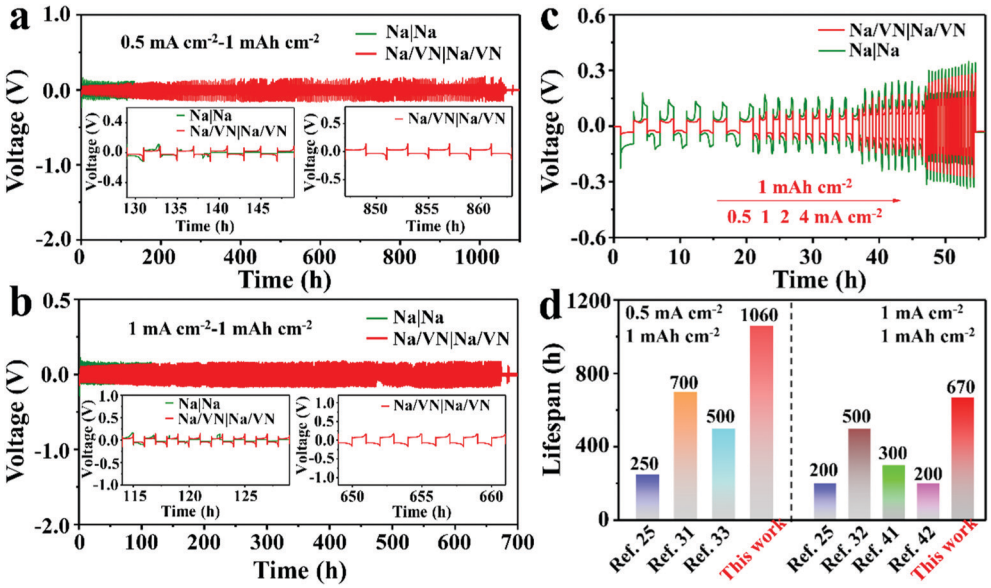

Fig. 2 Galvanostatic cycling of bare Na and Na/VN electrodes in symmetric cells (a) at 0.5 mA cm^{-2} with 1 mA h cm^{-2} and (b) at 1 mA cm^{-2} with 1 mA h cm^{-2}. (c) Rate performance of Na/VN and bare Na symmetric cells at various current densities of 0.5–4 mA cm^{-2}. (d) A comparison of the lifespan of Na/VN with the previously reported Na metal anodes.

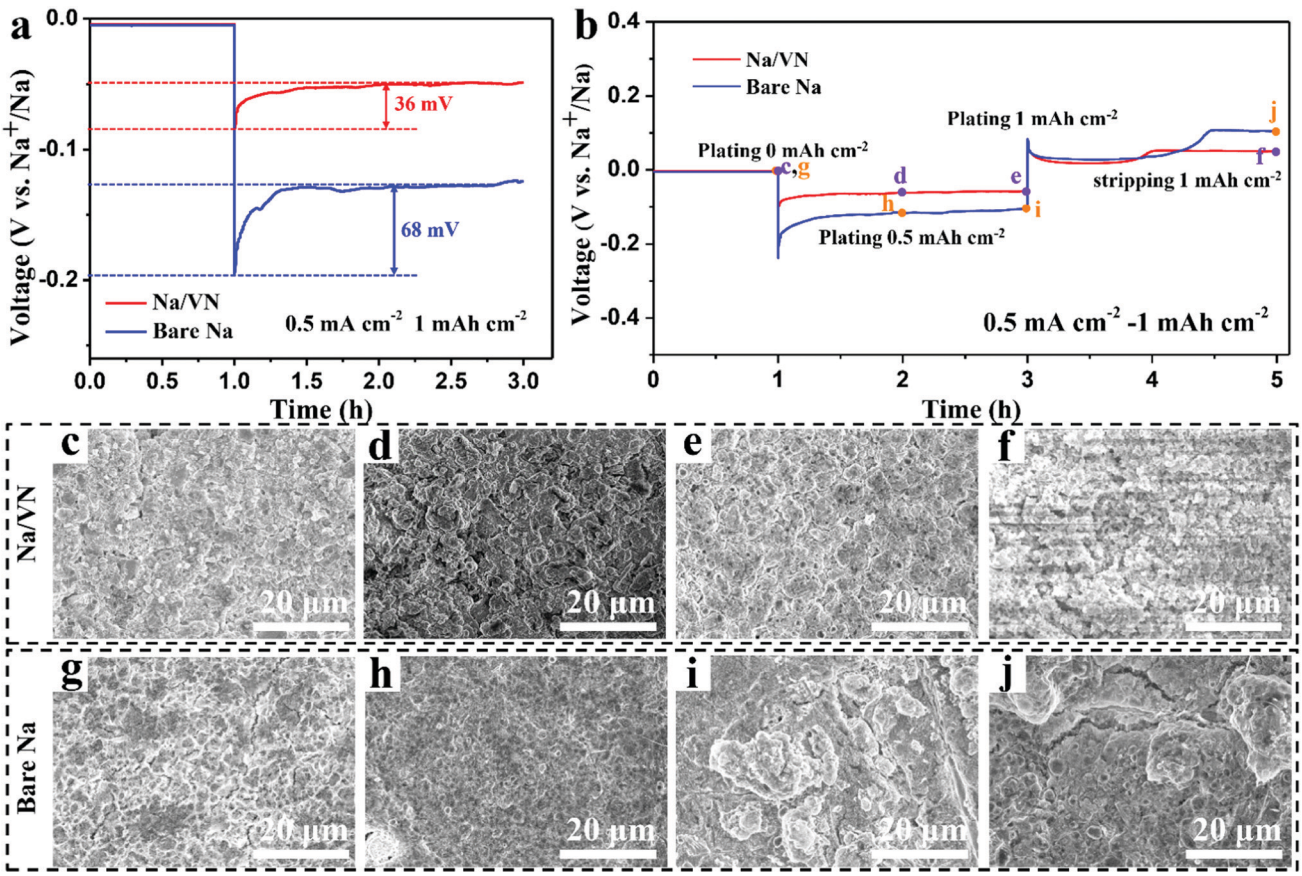

Fig. 3 (a) The nucleation overpotential of bare Na and Na/VN electrodes. (b) The first cycle of voltage–capacity profiles of Na plating on Na/VN and bare Na electrodes at 0.5 mA cm^{-2}. The top SEM view of Na plating on the Na/VN electrode (c–e) and bare Na electrode (g–i) with different plating capacities of 0, 0.5 and 1 mA h cm^{-2} at 0.5 mA cm^{-2}, respectively. The SEM images of (f) Na/VN and (j) the bare Na electrode after a stripping capacity of 1 mA h cm^{-2}.

 This journal is © The Royal Society of Chemistry 2022

Published on 30 May 2022. Downloaded on 8/22/2025 4:03:11 PM.

interlayer plays a vital role in realizing homogeneous deposition without dendrite formation. During the subsequent Na stripping, neither dendrites nor the bulk of ''dead Na'' can be observed on the Na/VN electrode (Fig. 3f and Fig. S10d, ESI†), indicating excellent reversibility. However, Fig. 3g–i and Fig. S11a–c (ESI†) demonstrate that the Na deposition on the bare Na electrode is nonuniform, leading to the formation of a rough deposition surface with ample bulk Na dendrites. Moreover, apparent cracks and plenty of bulk ''dead Na'' are displayed on the bare Na electrode when the plating Na is stripped (Fig. 3j and Fig. S11d, ESI†). Evidently, Na plating/stripping behaviour on the bare Na electrode is uncontrollable, which induces dendrites and ''dead Na'' formation, resulting in high polarized voltage and inferior cycling stability.

The Na deposition behaviors on the Na/VN and bare Na electrodes were also studied by *in situ* optical microscopy. As displayed in Fig. 4a, at the beginning of Na deposition at 0.5 mA cm^{-2}, the electrode of bare Na exhibits a smooth surface. Only after plating for 10 min, the electrode surface of bare Na grows ample mosslike dendrites. And with prolonging the plating time to 120 min, the mosslike dendrites cover the bare Na surface completely. With regard to the Na/VN, its surface still remains smooth even after continuously plating for 120 min (Fig. 4b), illustrating that the VN artificial interlayer facilitates the Na homogeneous deposition (Fig. S12, ESI†). Furthermore, for the symmetric cell after 10 cycles under 0.5 mA cm^{-2}/1 mA h cm^{-2}, plenty of remaining Na is apparent on the bare Na electrode, while the Na/VN electrode still maintains the initial state (silver gray and smooth surface) (Fig. S13, ESI†). The corresponding SEM images (Fig. 4c, d and Fig. S14, ESI†) also demonstrate that, after 10 cycles, ample cracks and Na dendrites are formed in the bare Na electrode,

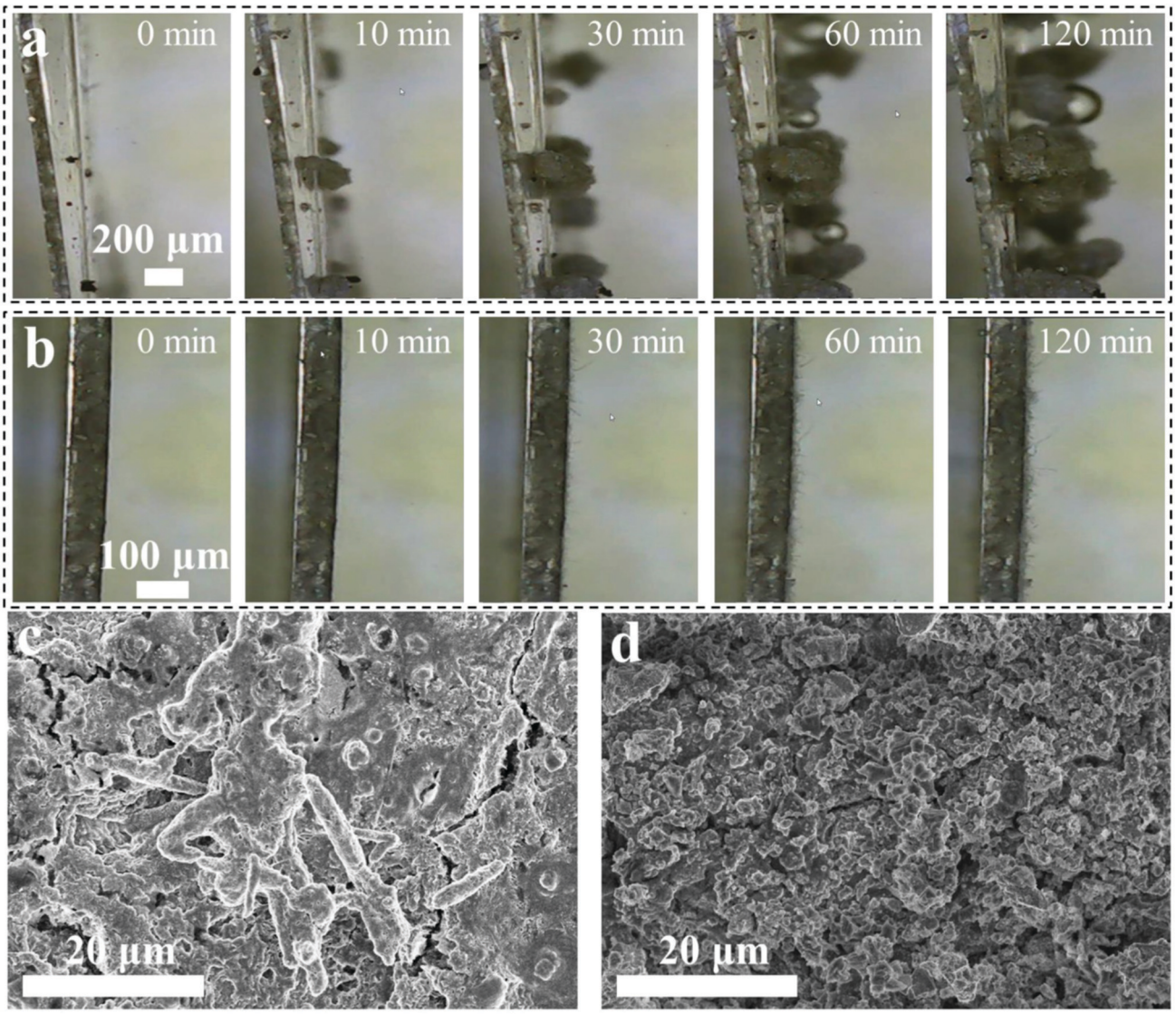

Fig. 4 The *in situ* optical photograph of the Na plating process on the surface of the (a) bare Na and (b) Na/VN electrode. The SEM images of the (c) bare Na and (d) Na/VN electrodes after 10 cycles at 0.5 mA cm^{-2} with 1 mA h cm^{-2}.

Published on 30 May 2022. Downloaded on 8/22/2025 4:03:11 PM.

and the VN artificial interlayer can stabilize the Na deposition/stripping with a dendrite-free morphology. Additionally, the structure stability of the VN interlayer after 10 cycles was further investigated by XRD and XPS analysis. The XRD reveals that the phase structure of the VN interlayer can be preserved completely (Fig. S15, ESI†). As seen from XPS spectra (Fig. S16, ESI†), it is clear that the V–N bond is still intact. The outstanding structure stability of the VN interlayer ensures the feasibility of long-term Na plating/stripping cycling.

To further understand the advantage of the artificial VN interlayer for Na deposition/stripping, DFT calculation was conducted. To clarify the adsorption ability of the artificial VN interlayer toward Na ions, four possibly stable Na^+ adsorption sites on the VN, including bridge, hollow, top on V and top on N sites, are studied, as shown in Fig. 5a–d and Fig. S17 (ESI†). The calculated adsorption energy of a Na atom on the bridge, hollow, top on V and top on N sites is −1.564, −1.457, −1.830 and −1.358 eV, respectively (Fig. 5e). Obviously, these adsorption energies are negative, and significantly less than that of bare Na (−0.860 eV),[45] indicating that the Na ion is inclined to adsorb and deposit on the VN surface. Furthermore, the charge differential density illustrations of the Na ion on various sites of the VN surface further reveal the strong chemical interaction and fast charge transfer between them (Fig. 5f–i and Fig. S18, ESI†). On the other hand, the Na deposition kinetics of the bare Na and Na/VN was examined. As clearly presented in Fig. S19 (ESI†), the bare Na symmetric cell exhibits a low exchange current density (0.068 mA cm^{-2}), suggesting a sluggish deposition kinetics. However, with the help of an artificial VN interlayer, the exchange current density increases to 0.215 mA cm^{-2}, indicating the improved charge transfer capacity for fast Na^+ deposition. And temperature-dependent electrochemical impedance spectroscopy (EIS) tests were employed to evaluate the activation energy for Na deposition. The EIS of symmetric Na/VN and bare Na cells after 10 cycles under 0.5 mA cm^{-2}/1 mA h cm^{-2} are presented in Fig. S20 (ESI†). The fitted curves consist of two semicircles, where the high frequency (first semicircle) corresponds to SEI

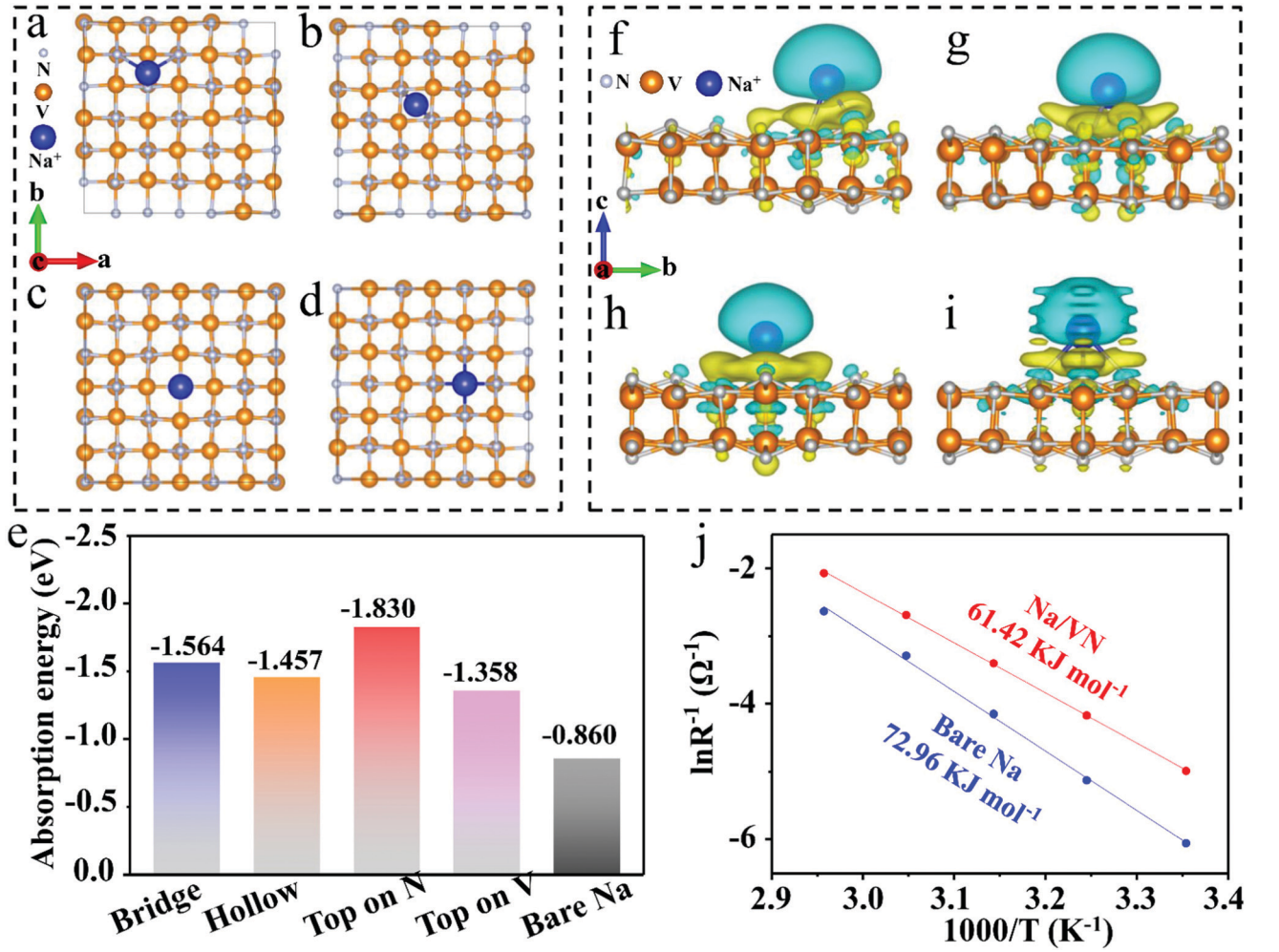

Fig. 5 Theoretical simulation. The top view of Na^+ adsorptions at (a) bridge, (b) hollow, (c) top on V and (d) top on N sites of the VN surface. (e) A comparison of adsorption energy. The front view of charge density differences for Na^+ adsorbing on the surface of VN at (f) bridge, (g) hollow, (h) top on V and (i) top on N sites. The yellow and cyan spheres represent electron accumulation and depletion, respectively. (j) The apparent activation energy required in symmetric bare Na and Na/VN cells.

 This journal is © The Royal Society of Chemistry 2022

Published on 30 May 2022. Downloaded on 8/22/2025 4:03:11 PM.

resistance (R_{SEI}) and the low frequency (second semicircle) is assigned to the charge transfer resistance (R_{ct}). Obviously, the bare Na electrode presents much higher R_{SEI} and R_{ct} values than those of the Na/VN electrode. According to the Arrhenius equation ($T/R_{ct} = A\exp(-E_a/RT)$),[46] the calculated E_a for Na^+ deposition on Na/VN is 61.42 kJ mol^{-1}, which is smaller than that of bare Na (72.96 kJ mol^{-1}) (Fig. 5j), suggesting the fast interfacial charge transfer kinetics for Na/VN. Based on the above results, it is clear that the artificial VN interlayer possesses high sodiophilicity and rapid charge transfer kinetics achieving uniform Na deposition.

Finally, full cells based on a Na/VN anode and commercial NVP cathode were developed. As exhibited in Fig. 6a, the NVP||Na/VN full cell presents an outstanding rate performance compared to that of NVP||bare Na. Although these two cells display similar specific capacities at low current densities (1–5C), the capacities of NVP||Na/VN at high rates are much higher. For example, at ultrahigh 50C, the reversible capacity of the NVP||Na/VN can reach as high as 54 mA h g^{-1}, while the full cell of NVP||bare Na failed completely. And the NVP||bare Na full cell presents a serious voltage step during the discharge process (Fig. S21a, ESI†). However, in the NVP||Na/VN full cell, the voltage step is hard to observe (Fig. 6b), indicating that introducing an artificial VN interlayer can significantly decrease the polarization and enhance the electrochemical reaction kinetics at the electrode/electrolyte interface.[38] Moreover, the NVP||Na/VN full cell displays an outstanding cycling lifespan (800 cycles) and ultrahigh capacity retention of 96% (98 mA h g^{-1}) even at 5C, while the NVP||bare Na decays rapidly to 89 mA h g^{-1} only after 180 cycles (Fig. 6c and Fig. S21b, ESI†). Fig. S21c (ESI†) exhibits their EIS curves after 100 cycles. The NVP||Na/VN displays obviously much lower charge transfer resistance than that of NVP||bare Na, indicating faster charge transfer kinetics with the help of the artificial VN interlayer. These results demonstrate that the Na/VN is an excellent candidate anode for SMBs.

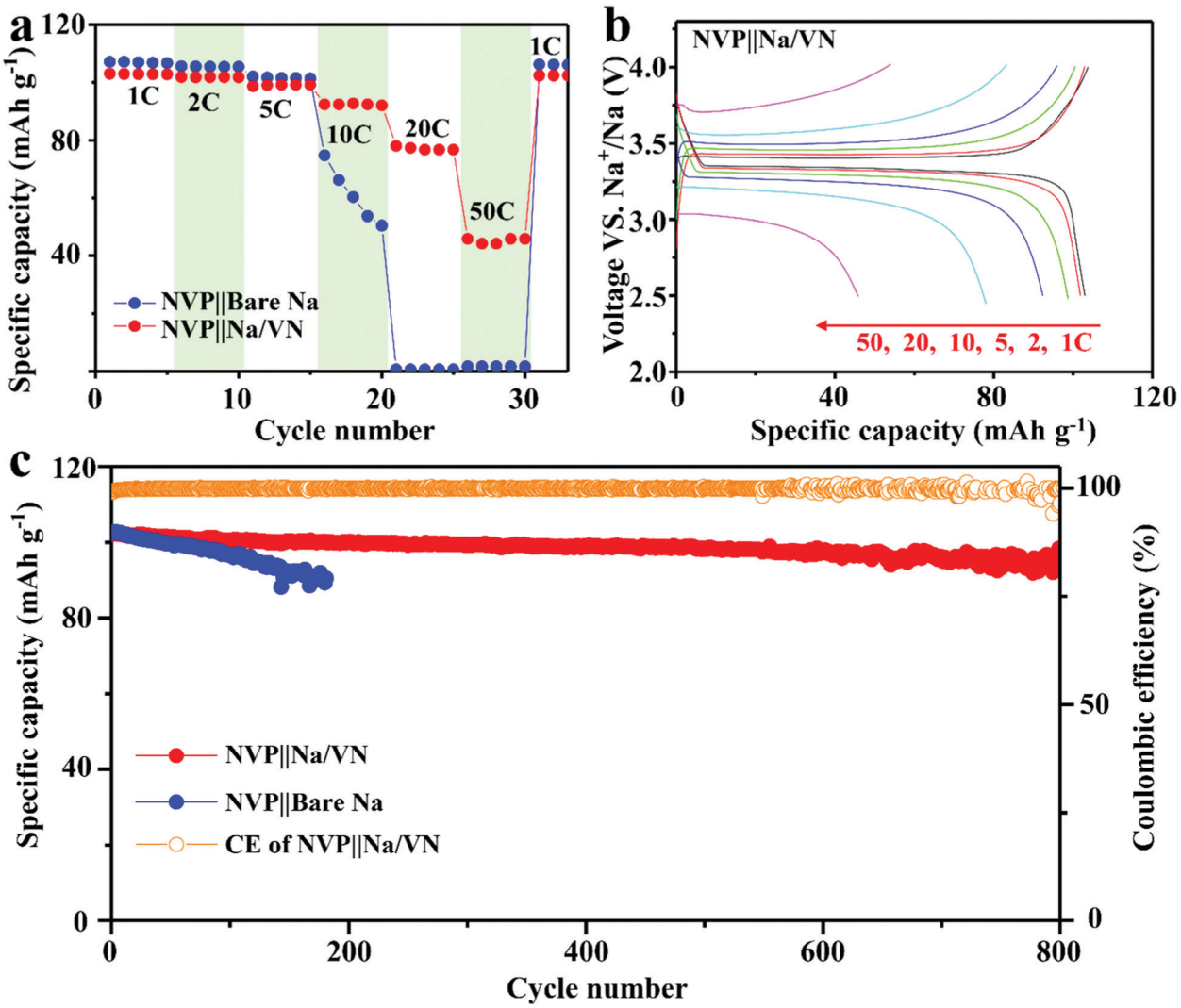

Fig. 6 (a) Rate performances ranging from 1 to 50C for the NVP||bare Na and NVP||Na/VN cells and (b) the charge–discharge curves of NVP||Na/VN. (c) The cycling stabilities of the NVP||bare Na and NVP||Na/VN cells at 5C.

Published on 30 May 2022. Downloaded on 8/22/2025 4:03:11 PM.

Conclusions

In summary, we designed an artificial VN interlayer to guide homogeneous Na nucleation and deposition. DFT calculations and experimental studies reveal that the VN interlayer not only possesses high sodiophilicity to manipulate uniform Na^+ nucleation and distribution on its surface during the plating process, but also displays high structure stability and fast charge transfer kinetics endowing rapid and effective plating/stripping cycling. As such, uniform Na deposition and dendrite-free morphology can be realized on the surface of the electrode modified by an artificial VN interlayer. Consequently, the Na/VN symmetric cell exhibits a prolonged cycling life over 1060 h (0.5 mA cm^{-2}) and 670 h (1 mA cm^{-2}), and then a high-performance full cell of NVP||Na/VN is developed. The sodiophilic VN interfacial layer provides a new opportunity for realizing dendrite-free, long lifespan and high-power-density of SMBs.

Conflicts of interest

There are no conflicts to declare.

Acknowledgements

The authors gratefully acknowledge the National Natural Science Foundation of China (Grant No. 51925207, U1910210, 51872277, 51972067, 51902062 and 52002083), the Fundamental Research Funds for the Central Universities (WK2060140026), the DNL cooperation Fund, CAS (DNL180310), the National Synchrotron Radiation Laboratory (KY2060000173), and the Guangdong Natural Science Funds for Distinguished Young Scholar (Grant No. 2019B151502039).

References

1 D. Lin, Y. Liu and Y. Cui, *Nat. Nanotechnol.*, 2017, **12**, 194–206.
2 C. Geng, W. Hua, D. Wang, G. Ling, C. Zhang and Q. H. Yang, *SusMat*, 2021, **1**, 51–65.
3 X. He, Y. Ni, Y. Li, H. Sun, Y. Lu, H. Li, Z. Yan, K. Zhang and J. Chen, *Adv. Mater.*, 2022, **1**, e2106565.
4 P. K. Nayak, L. Yang, W. Brehm and P. Adelhelm, *Angew. Chem., Int. Ed.*, 2018, **57**, 102–120.
5 S. Ye, L. Wang, F. Liu, P. Shi, H. Wang, X. Wu and Y. Yu, *Adv. Energy Mater.*, 2020, **10**, 2002647.
6 Y. Liu, Y. Zhai, Y. Y. Xia, W. Li and D. Y. Zhao, *Small Struct.*, 2021, **2**, 2000118.
7 Y. Wang, Z. Zhao, W. Zeng, X. Liu, L. Wang, J. Zhu and B. Lu, *J. Energy Chem.*, 2021, **58**, 292–299.
8 Y. Wu, L. Wu, S. Wu, Y. Yao, Y. Feng and Y. Yu, *Small Sci.*, 2021, **1**, 2100059.
9 C. Dong, Z. Lin, Y. Yin, Y. Qiao, W. Wang, Q. Wu, C. Yang, D. Rooney, C. Fan and K. Sun, *J. Energy Chem.*, 2021, **55**, 1–9.
10 F. N. Jiang, S. J. Yang, H. Liu, X. B. Cheng, L. Liu, R. Xiang, Q. Zhang, S. Kaskel and J. Q. Huang, *SusMat*, 2021, **1**, 506–536.
11 Y. Yang, C. Liu, Z. Lv, H. Yang, Y. Zhang, M. Ye, L. Chen, J. Zhao and C. C. Li, *Adv. Mater.*, 2021, **33**, e2007388.
12 X. Liu, Y. Li, X. Xu, L. Zhou and L. Mai, *J. Energy Chem.*, 2021, **61**, 104–134.
13 Z. Zhang, B. Xi, X. Ma, W. Chen, J. Feng and S. Xiong, *SusMat*, 2022, **2**, 114–141.
14 P. Shi, S. Zhang, G. Lu, L. Wang, Y. Jiang, F. Liu, Y. Yao, H. Yang, M. Ma, S. Ye, X. Tao, Y. Feng, X. Wu, X. Rui and Y. Yu, *Adv. Energy Mater.*, 2020, **11**, 2003381.
15 H. Shi, M. Yue, C. J. Zhang, Y. Dong, P. Lu, S. Zheng, H. Huang, J. Chen, P. Wen, Z. Xu, Q. Zheng, X. Li, Y. Yu and Z. S. Wu, *ACS Nano*, 2020, **14**, 8678–8688.
16 C. Bao, B. Wang, P. Liu, H. Wu, Y. Zhou, D. Wang, H. Liu and S. Dou, *Adv. Funct. Mater.*, 2020, **30**, 2004891.
17 Y. Xu, C. Wang, E. Matios, J. Luo, X. Hu, Q. Yue, Y. Kang and W. Li, *Adv. Energy Mater.*, 2020, **10**, 2002308.
18 X. Zheng, Z. Gu, X. Liu, Z. Wang, J. Wen, X. Wu, W. Luo and Y. Huang, *Energy Environ. Sci.*, 2020, **13**, 1788–1798.
19 W. Liu, P. Liu and D. Mitlin, *Chem. Soc. Rev.*, 2020, **49**, 7284–7300.
20 C. Chu, R. Li, F. Cai, Z. Bai, Y. Wang, X. Xu, N. Wang, J. Yang and S. Dou, *Energy Environ. Sci.*, 2021, **14**, 4318–4340.
21 H. Wang, E. Matios, J. Luo and W. Li, *Chem. Soc. Rev.*, 2020, **49**, 3783–3805.
22 X. Xia, C. F. Du, S. Zhong, Y. Jiang, H. Yu, W. Sun, H. Pan, X. Rui and Y. Yu, *Adv. Funct. Mater.*, 2021, **32**, 2110280.
23 H. Wang, E. Matios, C. Wang, J. Luo, X. Lu, X. Hu, Y. Zhang and W. Li, *J. Mater. Chem. A*, 2019, **7**, 23747–23755.
24 G. Wang, Y. Zhang, B. Guo, L. Tang, G. Xu, Y. Zhang, M. Wu, H. K. Liu, S. X. Dou and C. Wu, *Nano Lett.*, 2020, **20**, 4464–4471.
25 T. Yang, T. Qian, Y. Sun, J. Zhong, F. Rosei and C. Yan, *Nano Lett.*, 2019, **19**, 7827–7835.
26 S. Tang, Y. Y. Zhang, X. G. Zhang, J. T. Li, X. Y. Wang, J. W. Yan, D. Y. Wu, M. S. Zheng, Q. F. Dong and B. W. Mao, *Adv. Mater.*, 2019, **31**, e1807495.
27 H. Wang, Y. Wu, S. Liu, Y. Jiang, D. Shen, T. Kang, Z. Tong, D. Wu, X. Li and C. S. Lee, *Small Methods*, 2021, **5**, e2001050.
28 L. Mo, A. L. Chen, Y. Ouyang, W. Zong, Y. E. Miao and T. Liu, *ACS Appl. Mater. Interfaces*, 2021, **13**, 48634–48642.
29 J. Wang, R. Lian, S. Zhao, L. Zheng, Y. Huang, M. Wei, S. Mathur and Z. Hong, *Chem. Eng. J.*, 2022, **431**, 134272.
30 K. Lee, Y. J. Lee, M. J. Lee, J. Han, J. Lim, K. Ryu, H. Yoon, B. H. Kim, B. J. Kim and S. W. Lee, *Adv. Mater.*, 2022, **34**, e2109767.
31 Y. Xie, J. Hu, Z. Han, T. Wang, J. Zheng, L. Gan, Y. Lai and Z. Zhang, *Energy Storage Mater.*, 2020, **30**, 1–8.
32 B. Sun, P. Li, J. Zhang, D. Wang, P. Munroe, C. Wang, P. H. L. Notten and G. Wang, *Adv. Mater.*, 2018, **30**, 1801334.
33 Q. Li, Y. Chen, J. Zhang, W. Tian, L. Wang, Z. Ren, X. Ren, X. Li, B. Gao, X. Peng, P. K. Chu and K. Huo, *Nano Energy*, 2018, **51**, 128–136.
34 Y. Zhong, D. Chao, S. Deng, J. Zhan, R. Fang, Y. Xia, Y. Wang, X. Wang, X. Xia and J. Tu, *Adv. Funct. Mater.*, 2018, **28**, 1706391.
35 S. Wei, C. Wang, S. Chen, P. Zhang, K. Zhu, C. Wu, P. Song, W. Wen and L. Song, *Adv. Energy Mater.*, 2020, **10**, 1903712.
36 R. Saroha, J. H. Oh, Y. H. Seon, Y. C. Kang, J. S. Lee, D. W. Jeong and J. S. Cho, *J. Mater. Chem. A*, 2021, **9**, 11651–11664.

 This journal is © The Royal Society of Chemistry 2022

37 J. Yuan, X. Hu, J. Chen, Y. Liu, T. Huang and Z. Wen, *J. Mater. Chem. A*, 2019, **7**, 9289–9296.
38 A. Rudola, D. Aurbach and P. Balaya, *Electrochem. Commun.*, 2014, **46**, 56–59.
39 P. Li, T. Xu, P. Ding, J. Deng, C. Zha, Y. Wu, Y. Wang and Y. Li, *Energy Storage Mater.*, 2018, **15**, 8–13.
40 X. Zheng, P. Li, Z. Cao, W. Luo, F. Sun, Z. Wang, B. Ding, G. Wang and Y. Huang, *Small*, 2019, **15**, e1902688.
41 M. Guo, H. Dou, W. Zhao, X. Zhao, B. Wan, J. Wang, Y. Yan, X. Wang, Z. F. Ma and X. Yang, *Nano Energy*, 2020, **70**, 104479.
42 H. Wang, C. Wang, E. Matios and W. Li, *Nano Lett.*, 2017, **17**, 6808–6815.
43 M. Q. Zhu, S. M. Li, B. Li, Y. J. Gong, Z. G. Du and S. B. Yang, *Sci. Adv.*, 2019, **5**, eaau6264.
44 K. Yan, Z. Lu, H. W. Lee, F. Xiong, P.-C. Hsu, Y. Li, J. Zhao, S. Chu and Y. Cui, *Nat. Energy*, 2016, **1**, 16010.
45 Y. Jiang, Y. Yang, F. Ling, G. Lu, F. Huang, X. Tao, S. Wu, X. Cheng, F. Liu, D. Li, H. Yang, Y. Yao, P. Shi, Q. Chen, X. Rui and Y. Yu, *Adv. Mater.*, 2022, **34**, e2109439.
46 Y. Guo, P. Niu, Y. Liu, Y. Ouyang, D. Li, T. Zhai, H. Li and Y. Cui, *Adv. Mater.*, 2019, **31**, e1900342.

Published on 30 May 2022. Downloaded on 8/22/2025 4:03:11 PM.